J. Fluid Mech. (2013), *vol.* 719, *pp.* 82–96.
doi:10.1017/jfm.2012.631

The evolution of miscible gravity currents in horizontal porous layers

M. L. Szulczewski and R. Juanes†

Department of Civil and Environmental Engineering, Massachusetts Institute of Technology, Cambridge, MA 02139, USA

(Received 16 August 2012; revised 23 October 2012; accepted 16 December 2012)

Gravity currents of miscible fluids in porous media are important to understand because they occur in important engineering projects, such as enhanced oil recovery and geologic CO_2 sequestration. These flows are often modelled based on two simplifying assumptions: vertical velocities are negligible compared with horizontal velocities, and diffusion is negligible compared with advection. In many cases, however, these assumptions limit the validity of the models to a finite, intermediate time interval during the flow, making prediction of the flow at early and late times difficult. Here, we consider the effects of vertical flow and diffusion to develop a set of models for the entire evolution of a miscible gravity current. To gain physical insight, we study a simple system: lock exchange of equal-viscosity fluids in a horizontal, vertically confined layer of permeable rock. We show that the flow exhibits five regimes: (i) an early diffusion regime, in which the fluids diffuse across the initially sharp fluid–fluid interface; (ii) an S-slumping regime, in which the fluid–fluid interface tilts in an S-shape; (iii) a straight-line slumping regime, in which the fluid–fluid interface tilts as a straight line; (iv) a Taylor-slumping regime, in which Taylor dispersion at the aquifer scale enhances mixing between the fluids and causes the flow to continuously decelerate; and (v) a late diffusion regime, in which the flow becomes so slow that mass transfer again occurs dominantly though diffusion.

Key words: gravity currents, mixing and dispersion, porous media

1. Introduction

Gravity currents involving miscible fluids in porous layers occur in important engineering systems. For example, during the drilling of an oil well, miscible drilling fluids penetrate into the reservoir as a gravity current (Dussan & Auzerais 1993). Later in the life of some reservoirs, oil production is enhanced by injecting a miscible fluid such as CO_2 or a mixture of refined hydrocarbons, which migrates though the reservoir as a gravity current (Lake 1989). Along the coastline, seawater can infiltrate freshwater aquifers as a gravity current (Henry 1964). In deep saline aquifers, miscible gravity currents can occur during CO_2 sequestration when the CO_2 dissolves into the groundwater. Since groundwater with dissolved CO_2 is more dense than the ambient groundwater, it will migrate away from the free-phase CO_2 as a gravity current.

† Email address for correspondence: juanes@mit.edu

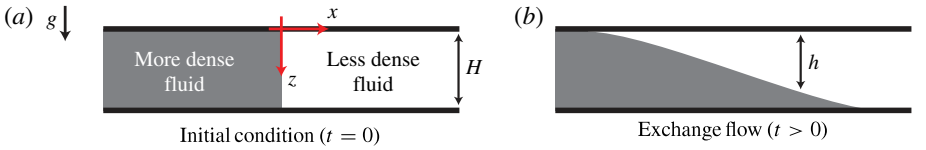

FIGURE 1. (Colour online) We study the lock exchange of two miscible, equal-viscosity fluids in a horizontal porous layer. (*a*) The lock gate is initially located at $x = 0$. The fluid on the left of the gate is more dense than the fluid on the right. (*b*) After the lock gate is removed, the fluids undergo an exchange flow.

Many models of gravity currents in porous media have been derived under several simplifying assumptions. One common assumption is that vertical flow velocities are negligible compared with horizontal velocities (Bear 1972; Yortsos 1995). This assumption is often called the Dupuit approximation or vertical-flow equilibrium. While diffusion and dispersion in porous-media flows have been studied extensively, gravity–current models commonly assume that these effects are negligible compared with advection (Bear 1972). This assumption is often called the sharp-interface approximation since neglecting diffusion and dispersion causes the fluids to always be separated by a sharp boundary. Under these assumptions, several models of gravity currents have been developed for two-dimensional rectilinear systems (Bear 1972; De Josselin De Jong 1981; Huppert & Woods 1995; Hesse *et al.* 2007; de Loubens & Ramakrishnan 2011; MacMinn, Szulczewski & Juanes 2011), two-dimensional axisymmetric systems (Barenblatt 1952; Dussan & Auzerais 1993; Lyle *et al.* 2005; Nordbotten & Celia 2006) and three-dimensional systems (Vella & Huppert 2006; de Loubens & Ramakrishnan 2011).

Recent work on seawater intrusion into coastal freshwater aquifers has included the effects of both vertical flow and diffusion or dispersion. Tartakovsky *et al.* (2004) incorporate linear dispersion through a perturbation analysis, Dentz *et al.* (2006) incorporate diffusion through a perturbation analysis and Paster & Dagan (2007) incorporate velocity-dependent transverse dispersion though a boundary-layer analysis. In these studies, the geologic setting makes the flow field steady state: the pressure-driven flow of freshwater toward the sea resists the gravity-driven flow of seawater into the aquifer, ultimately freezing the position of the seawater current. As a result, the incorporation of vertical flow and diffusion/dispersion does not affect the dynamics of the gravity–current propagation.

Here, we consider the effects of vertical flow and diffusion on gravity currents that do not exhibit a steady state. We study a simple system to gain physical insight: the lock exchange of equal-viscosity fluids in a horizontal, vertically confined layer of permeable rock (figure 1). The layer is infinite in the horizontal direction; the top and bottom of the layer are impermeable boundaries. Initially, the more dense fluid occupies the left half of the layer, and is separated by the lock gate from the less dense fluid on the right. When the gate is removed, the fluids undergo an exchange flow, with the more dense fluid flowing to the right along the bottom of the layer and the less dense fluid flowing to the left along the top.

Currently, the model for this system, which we call the straight-line slumping model, is based on both the Dupuit and sharp-interface approximations (Bear 1972; De Josselin De Jong 1981; Huppert & Woods 1995). While this model provides physical insight and can accurately describe the flow when the approximations hold, it is valid for only a finite, intermediate time interval during the flow. It is not valid at early times after the lock gate is removed because vertical velocities are important in the

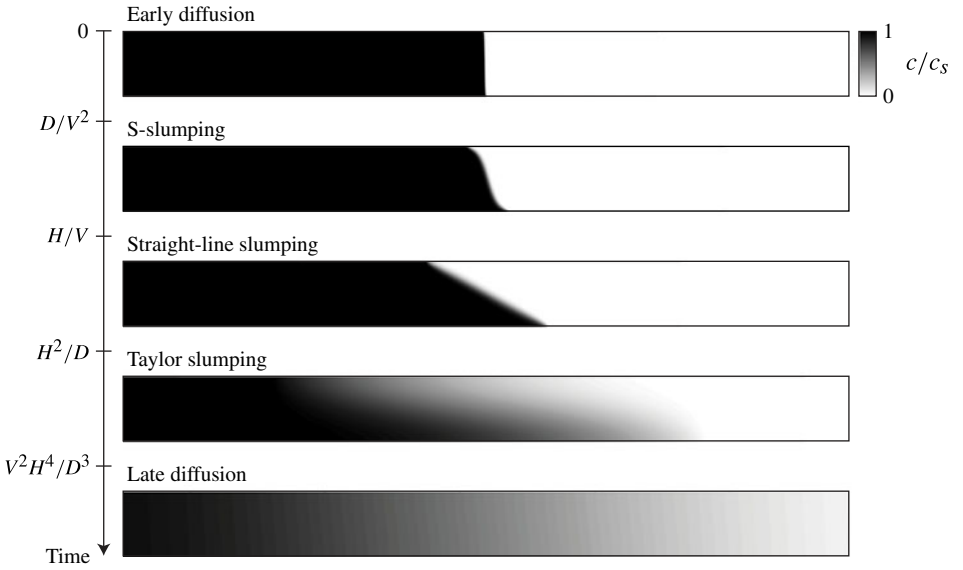

FIGURE 2. The flow evolves through the five self-similar regimes shown here by simulation results. The grey scale represents the concentration of the more dense fluid, c, normalized to the saturated concentration, c_s. The scalings of the transition times between the regimes are shown in terms of the layer thickness, H, the diffusion coefficient, D, and the characteristic velocity, $V = \Delta\rho g k/\mu\phi$. When $HV/D \lesssim 1$, the first and final transition times become equal, the duration of the intermediate regimes becomes zero, and lateral diffusion becomes the dominant mass transfer mechanism for all times.

early slumping. At late times, it is also not valid because diffusion and dispersion will eventually smear the sharp interface between the fluids into a large transition zone.

We find that the lock exchange of miscible fluids exhibits four self-similar regimes in addition to straight-line slumping (figure 2). For each regime, we simplify the governing equations to develop an analytical model of the flow. We find that neglecting vertical flow and diffusion is only valid at intermediate times during the straight-line slumping regime. For all other times, at least one of these effects must be included to capture the physics.

We validate the models of two of the regimes, S-slumping and straight-line slumping, with experiments. The experiments are performed in acrylic Hele-Shaw cells with a 3 mm gap that is packed with glass beads. The fluids are water and dyed salt water. To prepare an experiment, we first turn the cell upright so that the long dimension is vertical, fill it halfway with salt water, and then the rest of the way with fresh water so that the fresh water–salt water interface is horizontal. To begin the experiment, we turn the cell 90° and image the fluid interface with a DSLR camera.

We validate all of the models with numerical simulations of the full governing equations. When comparing the models with simulation results, we consider the vertically averaged concentration of the aquifer, $\bar{c}$. When the interface between the two fluids is sharp, this is directly proportional to the height of the more dense fluid: $\bar{c} \sim H - h$ (figure 1). We also consider the mass flux across the original location of the lock gate, which is a convenient parameter to characterize the system throughout its entire evolution, regardless of whether the fluid–fluid interface remains sharp or a large transition zone develops due to mixing.

2. Governing equations

The density-driven flow of two miscible fluids in a horizontal porous medium is described by a coupled system of equations. When the density difference between the fluids is small relative to the density of the fluids, the Boussinesq approximation is valid and the equations are (Landman & Schotting 2007):

$$\nabla \cdot \boldsymbol{u} = 0, \tag{2.1}$$

$$\boldsymbol{u} = -\frac{k}{\mu\phi}(\nabla p - \rho(c) g\hat{\boldsymbol{z}}), \tag{2.2}$$

$$\frac{\partial c}{\partial t} + \boldsymbol{u} \cdot \nabla c - D\nabla^2 c = 0. \tag{2.3}$$

Equation (2.1) expresses conservation of mass for the entire fluid mixture, equation (2.2) is Darcy's law and equation (2.3) is the concentration equation. The concentration, c, may be interpreted in two ways: if the two fluids are both solvents and the more dense fluid contains the dissolved component, such as the case for a water/salt water system, then c is the concentration of the dissolved component; if the two fluids are pure fluids such as water and ethanol, c is the concentration of the denser fluid. For convenience, we assume the former case in the remainder of the text. The density, ρ, is assumed to be a linear function of the concentration: $\rho = \rho_0 + \Delta\rho(c/c_s)$, where $\Delta\rho$ is the maximum density difference between the fluids and c_s is the saturated concentration ($c_s = 1$ for a system of two pure fluids). The remaining variables are as follows: $\boldsymbol{u} = (u, v)$ is the pore velocity, k is the permeability, μ is the dynamic viscosity, ϕ is the porosity, p is the pressure, g is the gravitational acceleration and D is the diffusion coefficient. For simplicity, we assume that hydrodynamic dispersion is negligible; we address the implications of this assumption in the conclusions. The initial conditions are that the velocity is zero everywhere, and that the more dense fluid is confined to the left half of the domain:

$$\boldsymbol{u}(x, z, t = 0) = \boldsymbol{0}, \quad c(x, z, t = 0) = \begin{cases} c_s & x \leqslant 0, \\ 0 & x > 0. \end{cases} \tag{2.4}$$

The boundary conditions and conditions at infinity are

$$v(z = 0, H) = u(x \to \pm\infty) = \left.\frac{\partial c}{\partial z}\right|_{z=0,H} = \left.\frac{\partial c}{\partial x}\right|_{x\to\pm\infty} = 0. \tag{2.5}$$

When the governing equations (2.1)–(2.3) are made dimensionless (see appendices A and B), there is only one governing parameter: the Rayleigh number, $Ra = \Delta\rho g k H/\mu\phi D$, which compares the strength of advection to diffusion.

We solve the governing equations using two methods. In the first method, we simplify the equations using scaling analyses or perturbation theory and solve the resulting equations analytically. In the second method, we solve the full, two-dimensional system of equations numerically. We integrate in space using finite volumes with linear reconstructions and the MC limiter (LeVeque 2002). We integrate in time using Runge–Kutta methods (Lambert 1991). For short-time simulations, we use an explicit, two-stage method; for longer simulations, we switch to an implicit–explicit two-stage method to remove the time step restriction from the diffusion term (Ascher, Ruuth & Spiteri 1997). The numerical scheme is second-order accurate in both space and time. We have confirmed that the numerical results are converged, grid-independent results.

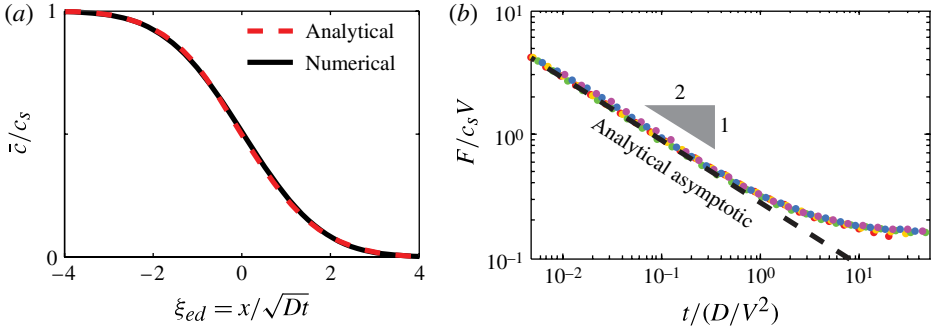

FIGURE 3. (Colour online) (*a*) The analytical solution for the vertically averaged concentration ($\bar{c}/c_s$) (3.1) during the first regime, early diffusion, agrees well with the numerical profile (numerical data from $Ra = 500$). (*b*) The analytical flux, F/c_sV, across the original position of the lock gate (dashed, (3.2)) also agrees well with numerical results (circles; $Ra = 100, 200, 500, 700, 1200$), but specifically in the limit that time, t, approaches zero because the regime is an asymptotic. The simultaneous departure of all numerical data from the analytical solution shows that the transition time to the next regime scales as $t_{ss} \sim D/V^2$.

3. Flow regimes

3.1. *Early diffusion (ed)*

Immediately after the lock gate is removed, lateral diffusion across the vertical fluid–fluid interface dominates the mass flux. Diffusion dominates initially because, by Fick's law, the diffusive flux is proportional to the concentration gradient and therefore goes to infinity in the limit of an initially sharp interface. Since the dynamics involve only diffusion and the geometry is simple, this regime may be modelled by a similarity solution to a one-dimensional diffusion equation (Crank 1980):

$$\frac{c}{c_s} = \frac{1}{2}\left(1 - \mathrm{erf}\left(\frac{x}{2\sqrt{Dt}}\right)\right), \tag{3.1}$$

where the similarity variable is $\xi_{ed} = x/\sqrt{Dt}$. This equation agrees with numerical results for the vertically averaged concentration (figure 3*a*). The mass flux across the initial position of the gate is

$$F_{ed} = \frac{c_s}{2}\left(\frac{D}{\pi t}\right)^{1/2}, \tag{3.2}$$

which also agrees well with numerical results (figure 3*b*). Both of these expressions are valid in the limit $Ra \to 0$ or, for finite Rayleigh numbers, in the limit $t \to 0$, as shown graphically in figure 3(*b*) and analytically in appendix A. Equating the flux with the flux in the next regime, S-slumping, shows that the transition time to the next regime is $t_{ss} = 2.3D/V^2$, where $V = \Delta\rho g k/\mu\phi$.

3.2. *S-slumping (ss)*

In the second regime, the fluid–fluid interface tilts in an S-shaped curve. While the interface is diffuse for all finite Ra, we model the flow in the limit $Ra \to \infty$ for which the interface is sharp. In this limit, the problem is simplified because diffusion is negligible and the flow self similar in the variable $\xi_{ss} = x/Vt$, as shown by numerical results in figure 4(*a*).

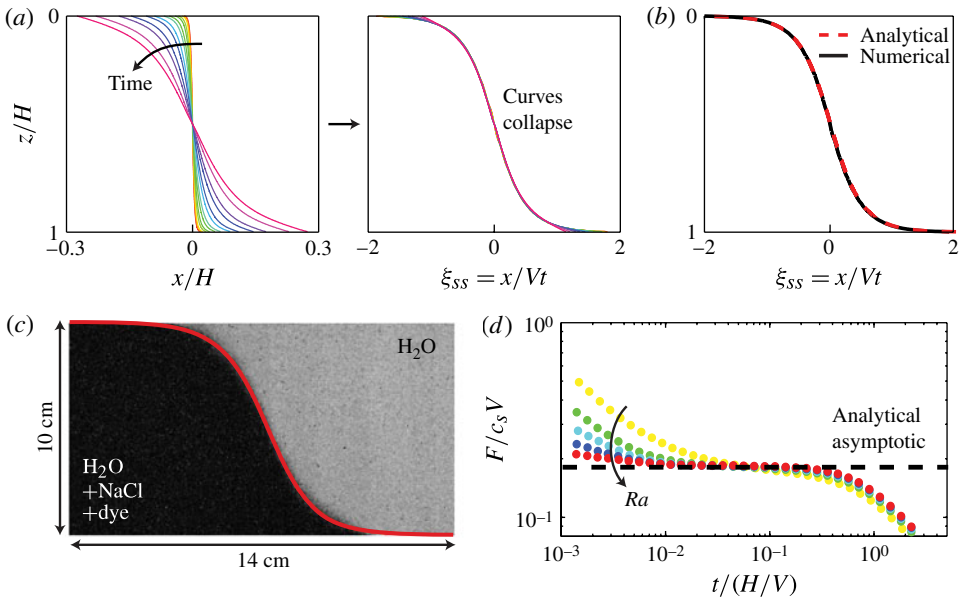

FIGURE 4. (Colour online) (*a*) The second regime, S-slumping, is self-similar in $\xi_{ss} = x/Vt$: when numerical solutions for the fluid–fluid interface at several times are plotted versus ξ_{ss}, they all collapse onto a single curve. (*b*) The approximate analytical solution for the height of the sharp interface (dashed line, shown in red in the online version; (3.3)) agrees well with numerical results for the problem with no diffusion (black; $Ra = \infty$). (*c*) The approximate solution (shown in red in the online version) also agrees well with experiments of salt water slumping in a Hele-Shaw cell packed with glass beads ($\Delta\rho = 50\ \mathrm{kg\ m^{-3}}$; bead diameter 0.5 mm; $t = 3$ min). (*d*) The analytical solution is an asymptotic in the limit $Ra \to \infty$: as Ra becomes larger, the mass flux calculated from numerics (circles; $Ra = 300, 1000, 2150, 4650, 10\,000$) converges to the value from the analytical solution (dashed). The transition time to the next regime scales as $t_{sls} \sim H/V$, as shown by the simultaneous departure of all numerical data from the dashed line.

While there is no exact, analytical model for the flow in this regime, the expression for the similarity variable provides physical insight into the flow. Rearranging the expression for ξ_{ss} to solve for x and differentiating with respect to time yields an expression for the lateral velocity of the interface: $u = \xi_{ss} V$, where ξ_{ss} may now be interpreted as a function of the scaled interface height, h/H. For example, at the leading edge of the current where $h/H = 1$, figure 4(*a*) shows that $\xi_{ss} \approx 1.5$, so the velocity of the leading edge is $u \approx 1.5V$. This expression indicates that the interface advances at a constant rate in time. It also indicates that the aquifer height, H, does not affect the dynamics: in other words, the velocity field in two aquifers of different heights is exactly the same when the vertical dimension is scaled by H.

To develop an approximate model of the flow, we integrate the velocity along the interface at $t = 0$, found analytically by De Josselin De Jong (1981). The solution for the height of the interface of the less dense fluid, h, is (see figure 1):

$$\frac{h}{H} = \frac{2}{\pi}\mathrm{arccot}(\mathrm{e}^{-\pi x/Vt}). \tag{3.3}$$

This solution agrees well with both numerical and experimental results (figure 4*b,c*). From this equation, we find the mass flux as the time rate of change of the dissolved species mass on the right-hand side of the lock gate:

$$F_{ss} = \frac{1}{H}\frac{\mathrm{d}}{\mathrm{d}t}\left(c_s \int_0^\infty (H-h)\,\mathrm{d}x\right) = 0.186 c_s V. \tag{3.4}$$

We use the similarity variable to simplify the integral and then evaluate it numerically. Since (3.3) and (3.4) were derived in the limit $Ra \to \infty$, they are asymptotics, accurately describing the flow at large Rayleigh numbers but becoming increasingly inaccurate for small Ra (figure 4*d*). In the limit $Ra \to \infty$, they are rigourously valid for an infinitesimally small time after $t = 0$ since they are derived using only the velocity field at $t = 0$, but they provide reasonable descriptions of the flow for longer times (figure 4*c,d*). For finite Ra, they become valid at the onset of the S-slumping regime at time $t_{ss} = 2.3D/V^2$.

3.3. *Straight-line slumping (sls)*

In the third regime, the fluid–fluid interface tilts as a straight line. As in the previous regime, the interface is diffuse, but we model the flow in the sharp-interface limit. Since the lateral extent of the flow in this regime is typically large compared with the aquifer thickness, we assume that vertical velocities are negligible compared with horizontal velocities (Dupuit approximation is valid). Under these approximations, Huppert & Woods (1995) showed that the flow is self-similar in the variable $\xi_{sls} = x/\sqrt{VHt}$, and derived the following analytical solution for the interface height, h:

$$\frac{h}{H} = \frac{1}{2}\left(1 + \frac{x}{\sqrt{VHt}}\right). \tag{3.5}$$

This solution agrees well with both numerical and experimental results (figure 5*a,b*). Perturbation analysis shows that this solution is accurate to first order in $\varepsilon = H/L$, where L is the horizontal extent of the interface (Yortsos 1995).

As in the previous regime, the expression for the similarity variable, $\xi_{sls} = x/\sqrt{VHt}$, provides physical insight into the flow. Interpreting VH as analogous to a diffusion coefficient, we find that ξ_{sls} exhibits the same form as the similarity variable for Fickian diffusion alone, $\xi_{ed} = x/\sqrt{Dt}$. This comparison indicates that the fluid interface in this regime spreads diffusively. Specifically, the lateral velocity of the interface, u, decreases in time as $u \sim t^{-1/2}$, just as the velocity of a concentration contour decreases as $t^{-1/2}$ as it propagates away from the initially vertical interface in the early diffusion regime. The exact expression for the flow velocity can be determined from (3.5): $u = (h/H - 1/2)\,(VH/t)^{1/2}$. This diffusive spreading is different from the S-slumping regime, in which the lateral velocities are constant in time. It is also different because the aquifer thickness, H, now affects the dynamics through the effective diffusion coefficient $D_{sls} = VH$. Since the spreading is diffusive, the mass flux across the initial lock position is also diffusive:

$$F_{sls} = \frac{1}{H}\frac{\mathrm{d}}{\mathrm{d}t}\left(c_s \int_0^{x_n} (H-h)\,\mathrm{d}x\right) = \frac{c_s}{8}\left(\frac{VH}{t}\right)^{1/2}, \tag{3.6}$$

where $x_n = \sqrt{VHt}$ is the location of the rightmost edge of the dense current.

Since the equations for the flux (3.6), velocity and interface height (3.5) are based on the sharp-interface approximation, they represent asymptotics of the full problem

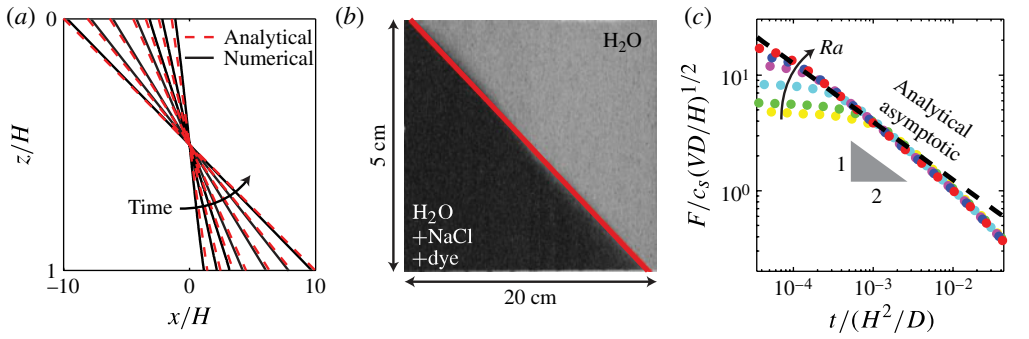

FIGURE 5. (Colour online) (*a*) The analytical model in the third regime, straight-line slumping, for the height of the sharp interface (dashed line, show in red in the online version; (3.5)) matches the numerical solution for the problem with no diffusion (black; $Ra = \infty$; $t/(H/V) = 2, 6, 12, 20, 40, 65, 99$). Since the model is an intermediate asymptotic (Barenblatt 1996), the disagreement is largest at early times and decreases as $t \to \infty$. (*b*) The analytical model (shown in red in the online version) also agrees well with experiments of salt water slumping in a Hele-Shaw cell packed with glass beads ($\Delta\rho = 100\,\mathrm{kg\,m^{-3}}$; bead diameter 0.5 mm; $t = 10$ min). (*c*) Since the model is based on the sharp-interface approximation, the mass flux, F, calculated from numerics (circles; $Ra = 300, 700, 1000, 2150, 4650, 10\,000$) approaches the flux from the model (dashed; (3.5)) as $Ra \to \infty$. The departure of all numerical data from the dashed line shows that the transition time to the next regime scales as $t_{Ts} \sim H^2/D$.

with diffusion, providing an increasingly accurate description of the flow as $Ra \to \infty$ (figure 5). They become invalid at time $t_{Ts} \sim H^2/D$, when the regime ends because vertical diffusion creates a broad transition zone between the two fluids.

3.4. *Taylor slumping (Ts)*

In the fourth regime, the dynamics are controlled by the coupling between diffusion and gravity-driven advection. Advection impacts diffusion because it increases the interfacial area between the two fluids, which accelerates the diffusive mixing. This process is Taylor dispersion at the aquifer scale, for which the regime is named (Taylor 1953). Diffusive mixing impacts advection because it reduces the lateral density gradient that drives advection. The relationship between the gradient of vertically averaged density, $\overline{\rho}$, and the lateral velocity, u, is

$$u(z) = \frac{gkH}{\phi\mu}\frac{\partial\overline{\rho}}{\partial x}\left(\frac{1}{2} - \frac{z}{H}\right) + O(\varepsilon^2), \tag{3.7}$$

where $\varepsilon = H/L$ and L is the horizontal extent of the flow (B 6). This equation shows that at long times when $\varepsilon \ll 1$, mixing retards the gravity-driven slumping in direct proportion to the degree to which it reduces $\partial\overline{\rho}/\partial x$.

To model Taylor slumping, we derive an equation for the vertically averaged concentration, $\overline{c}$ (see appendix B):

$$\frac{\partial\overline{c}}{\partial t} - D\frac{\partial^2\overline{c}}{\partial x^2} - \frac{\partial}{\partial x}\left(\frac{H^4V^2}{120Dc_s^2}\left[\frac{\partial\overline{c}}{\partial x}\right]^2\frac{\partial\overline{c}}{\partial x}\right) = 0. \tag{3.8}$$

The middle term in this equation captures Fickian diffusion in the lateral direction. The rightmost term captures Taylor slumping. This type of term involving the

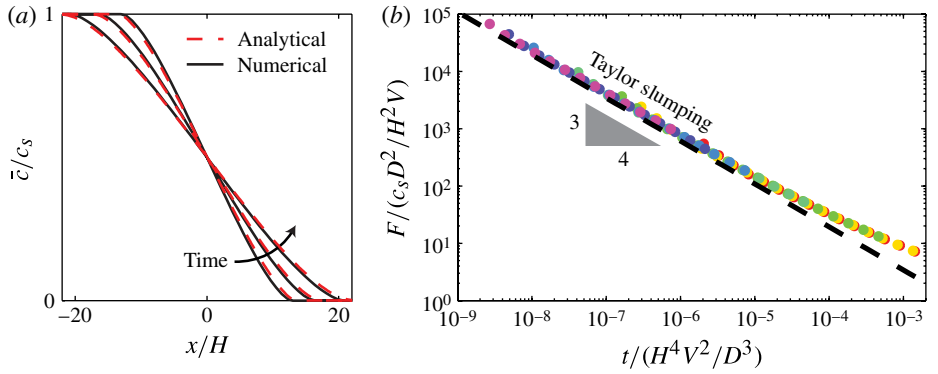

FIGURE 6. (Colour online) (*a*) The analytical model for the vertically averaged concentration ($\bar{c}/c_s$) during the Taylor slumping regime (3.10) agrees well with the numerical profile ($Ra = 1000$; $t/(H/V) = 670, 1700, 4500$). (*b*) The mass flux ($F/(c_sD^2/H^2V)$) obtained from this model (dashed, (3.11)) also agrees well with numerical results (circles; $Ra = 300, 700, 1000, 2150, 4650, 10\,000$). Here we only show data after the onset of Taylor slumping for clarity. The transition time to the next regime is $t_{ld} \sim H^4V^2/D^3$, as shown by the simultaneous departure of all data from the dashed line.

concentration gradient cubed occurs in a variety of models describing the coupling between buoyancy and shear dispersion, including models of pipe flow (Erdogan & Chatwin 1967) and open-channel flow (Smith 1976).

To emphasize the physical meaning of the Taylor slumping term, we compare it with the classical Taylor dispersion term for Poiseuille flow between parallel plates. In this system, the equation for the vertically averaged concentration is

$$\frac{\partial \bar{c}}{\partial t} + \bar{u}\frac{\partial \bar{c}}{\partial x} - D\frac{\partial^2 \bar{c}}{\partial x^2} - \frac{\partial}{\partial x}\left(\frac{b^2\bar{u}^2}{210D}\frac{\partial \bar{c}}{\partial x}\right) = 0 \tag{3.9}$$

where $\bar{u}$ is the average velocity and b is the distance between the plates (Nguyen 2011). The rightmost term in this equation captures classical Taylor dispersion. It is a linear diffusion term with an effective diffusion coefficient $D_{Td} = b^2\bar{u}^2/210D$. The Taylor slumping term in (3.8) can also be interpreted as a diffusion term, but it is nonlinear with an effective diffusion coefficient $D_{Ts} = (H^4V^2/120Dc_s^2)\,(\partial \bar{c}/\partial x)^2$. The nonlinearity arises due to the coupling between diffusive mixing and the gravity-driven flow: diffusive mixing reduces the flow velocity (3.7), which in turn reduces the diffusive mixing by lowering the rate at which the interfacial area between the two fluids grows. This coupling does not occur in classical Taylor dispersion because the velocity is constant during Poiseuille flow.

In (3.8), the Taylor slumping term dominates the Fickian diffusion term at early times when the aspect ratio of the flow is small relative to the Rayleigh number: $L/H \ll Ra/\sqrt{120}$. This result comes from scaling x by the lateral extent of the flow, L, and taking the ratio of the coefficients of the Taylor slumping term and Fickian diffusion term. When the Taylor slumping term dominates, the Fickian diffusion term may be neglected and the equation admits an exact, analytical similarity solution in the variable $\xi_{Ts} = x/\left(H^4V^2t/120D\right)^{1/4}$:

$$\frac{\bar{c}}{c_s} = \frac{1}{2} - \frac{1}{2\sqrt{12}}\left[\xi_{Ts}\left(\alpha^2 - \xi_{Ts}^2\right)^{1/2} + \alpha^2 \arcsin\left(\frac{\xi_{Ts}}{\alpha}\right)\right], \tag{3.10}$$

where $\alpha = (48/\pi^2)^{1/4}$. This solution agrees well with numerical results (figure 6*a*).

In Taylor slumping, the lateral velocities decrease subdiffusively in time, scaling as $u \sim t^{-3/4}$. Based on the similarity variable, the expression for the lateral velocity is $u = \xi_{Ts}\,(H^4V^2/480Dt^3)^{1/4}$, where ξ_{Ts} can now be interpreted as a function of the average concentration. For example, at the leading edge of the current where the average concentration is zero, $\xi_{Ts} = \alpha$ and $u = \alpha\,(H^4V^2/480Dt^3)^{1/4}$. The velocity decreases faster than in the previous regime, in which velocity decreases diffusively in time, due to the reduction in velocity caused by diffusive mixing (3.7).

Since the velocities are subdiffusive, the mass flux during Taylor slumping is also subdiffusive:

$$F_{Ts} = \frac{1}{H}\frac{\mathrm{d}}{\mathrm{d}t}\left(H\int_0^\infty \bar{c}\,\mathrm{d}x\right) = \frac{c_s}{\left(3240\pi^6\right)^{1/4}}\left(\frac{H^4V^2}{Dt^3}\right)^{1/4}. \tag{3.11}$$

This expression agrees well with numerical results (figure 6*b*), helping to validate the Taylor slumping model.

3.5. *Late diffusion (ld)*

At times much later than $t_{ld} = 2H^4V^2/405\pi^4D^3$, the Taylor slumping term in (3.8) becomes negligible compared with the Fickian diffusion term. This can been seen by comparing the fluxes due to Taylor slumping (3.11) and Fickian diffusion (3.2). At these late times, the vertically averaged density gradient, which drives the flow, becomes very small and causes the horizontal flow to become very slow (3.7). When the horizontal flow becomes slow, the vertical mass transfer due to diffusion dominates the horizontal mass transfer due to the flow, and the concentration becomes nearly uniform in the vertical direction. The relationship between the vertical concentration gradient and the horizontal velocity can be found explicitly from a perturbation analysis (B 7): $\partial c/\partial z = (1/D)(\partial\bar{c}/\partial x)\int_0^z u\,\mathrm{d}z + O(\varepsilon^2)$. As a result of the slow flow and nearly complete vertical mixing, mass transfer occurs dominantly via Fickian diffusion in the lateral direction. This regime is the same as the first regime, early diffusion, and may be modelled by (3.1).

For some conditions, the late diffusion regime occurs immediately after the early diffusion regime and there is no distinction between them. Subtracting the end time of the early diffusion regime from the onset time of the late diffusion regime yields an expression for the duration of the intermediate regimes: $t_{ld} - t_{ss} = 2D/405\pi^4V^2(Ra^4 - 2.3)$. When $Ra \lesssim 1$, the duration is zero and the two diffusion regimes occur consecutively.

4. Conclusion

The gravity-driven flow of two miscible fluids in a horizontal porous layer evolves through five regimes. When the fluids are initially separated by a sharp interface, the first regime is diffusion. In the next two regimes, the gravity-driven flow dominates. At the beginning of the flow, when the lateral extent of the current is less than the aquifer thickness, the fluid–fluid interface tilts in an S-shaped curve. In this regime, the leading edge of the interface propagates at a constant velocity. When the extent of the current exceeds the aquifer thickness, the fluid interface changes from an S-shaped curve to a straight line. In this regime, the leading edge continually decelerates, exhibiting a diffusive scaling in time. In the following regime, Taylor slumping, the flow becomes coupled to diffusive mixing. The flow affects diffusive mixing via Taylor

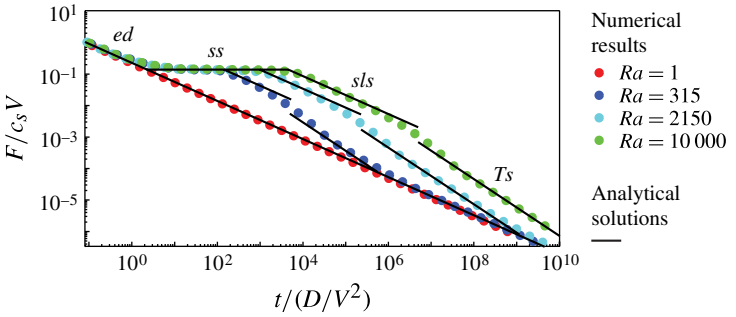

FIGURE 7. (Colour online) The entire evolution of the miscible lock-exchange problem in a horizontal porous layer may be described by combining analytical solutions for five flow regimes.

dispersion at the aquifer scale, in which the non-uniform flow velocities elongate the fluid–fluid interface over which diffusion acts to mix the fluids. Diffusive mixing affects the flow by reducing the lateral density gradient that drives the flow. This coupling causes the flow to decelerate subdiffusively. Eventually, the velocity becomes so low that diffusion causes the fluids to be nearly completely mixed in the vertical direction. In this regime, lateral diffusion through the aquifer again becomes the dominant mass transfer process. All of these regimes can be described by analytical models, which when combined in series, provide a complete picture of the entire evolution of the flow, as shown in figure 7.

The evolution of the flux is indicative, for example, of the rate of dissolution that can be expected from CO_2 injected and stored in geological traps. In geological CO_2 sequestration, relevant values of Ra exhibit a large range due to the large ranges of aquifer thickness and permeability (Ennis-King & Paterson 2005; Riaz *et al.* 2006). Assuming $\Delta\rho = 5$ kg m^{-3}, $k = 10$–1000 mD, $\mu = 1$ m Pas, $\phi = 0.2$, $H = 25$–500 m, $D = 1 \times 10^{-9}$ m^2 s$^-$, Ra ranges from $\sim$500 to over 1 million (Szulczewski *et al.* 2012): a range for which it is likely that all five regimes will play a role (figure 7).

While the models have been derived under the assumption of negligible hydrodynamic dispersion, four of the five models remain valid even in systems with strong dispersivity. Dispersion will not affect the first and final regimes in which lateral Fickian diffusion dominates, because the flow velocities are negligibly small in these regimes, which in turn makes hydrodynamic dispersion negligibly small. It will also not affect the models of S-slumping or straight-line slumping, since these models are based on the assumption of negligible fluid mixing. These models will still be valid at early times for which advection dominates diffusion and dispersion, although the timespan over which they are valid will likely be reduced since dispersion would cause the fluids to mix more rapidly.

While hydrodynamic dispersion will not affect most of the regimes, it will affect Taylor slumping since this regime describes the interplay between fluid mixing and gravity-driven advection. As a result, the model for Taylor slumping will be accurate in very slow flows for which dispersion is negligible. If dispersion is not negligible, the physical mechanism captured by the Taylor slumping model will likely still be valid: mixing will lead to a reduced lateral density gradient, which will decrease the horizontal velocity until lateral diffusion dominates the mass transfer. Hydrodynamic dispersion, however, will likely accelerate this process by enhancing the mixing.

Acknowledgements

This work was funded by the Cooperative Agreement between the Masdar Institute of Science and Technology (Masdar Institute), Abu Dhabi, UAE and the Massachusetts Institute of Technology (MIT), Cambridge, MA, USA, Reference No. 196F/002/707/102f/70/9374. Additional funding was provided by a Martin Fellowship for Sustainability (to MLS).

Appendix A. Early diffusion

To derive the model for the early diffusion regime, we scale the variables as follows:

$$\left.\begin{array}{llll} z = H\zeta, & x = L\eta, & t = (H^2/D)\tau, & p = \overline{P}p' + \rho_0 gH\zeta, \\ c = c_s c', & v = Vv', & u = Vu', & \end{array}\right\} \tag{A 1}$$

where $\overline{P} = \Delta\rho gH$ is the characteristic pressure and $V = \Delta\rho gk/\mu\phi$ is the characteristic velocity. We define a similarity variable, $\xi_{ed} = \eta/\sqrt{\tau}$. The scaled concentration equation (2.3) is then

$$-\frac{\xi_{ed}}{2}\frac{\partial c'}{\partial \xi_{ed}} + \tau^{1/2} Ra \frac{\partial}{\partial \xi_{ed}}(u'c') + \tau Ra \frac{\partial}{\partial \zeta}(w'c') - \frac{\partial^2 c'}{\partial \xi_{ed}^2} - \tau \frac{\partial^2 c'}{\partial \zeta^2} = 0. \tag{A 2}$$

In the limit $\tau \to 0$, it reduces to

$$\frac{\xi_{ed}}{2}\frac{\mathrm{d}c'}{\mathrm{d}\xi_{ed}} + \frac{\mathrm{d}^2 c'}{\mathrm{d}\xi_{ed}^2} = 0. \tag{A 3}$$

This equation is also obtained in the limit $Ra \to 0$ since the initial condition and boundary conditions make $\partial^2 c'/\partial\zeta^2 = 0$ for all times. The equation is the self-similar form of a one-dimensional diffusion equation in a laterally infinite domain. The solution is given in (3.1).

Appendix B. Taylor slumping

To derive the model for Taylor slumping, we vertically average the concentration equation (2.3)

$$\frac{\partial \overline{c}}{\partial t} + \frac{\partial}{\partial x}\overline{uc} - D\frac{\partial^2 \overline{c}}{\partial x^2} = 0, \tag{B 1}$$

where overbars denote vertical averages (e.g. $\overline{c} = 1/H\int_0^H c\,\mathrm{d}z$). We then obtain an expression for the average advective flux, $\overline{uc}$, via a perturbation analysis of both the averaged and unaveraged governing equations. We begin the perturbation analysis by scaling the variables as follows:

$$\left.\begin{array}{llll} z = H\zeta, & x = L\xi, & p = \overline{P}p' + \rho_0 gH\zeta, & c = c_s c', \\ v = Vv', & u = Uu', & t = T\tau, & \end{array}\right\} \tag{B 2}$$

where $V = \Delta\rho gk/\mu\phi$, $U = \varepsilon V$, $P = \Delta\rho gH$ and $T = L/U$. Here $\varepsilon = H/L$, where L is the lateral extent of the flow, which is unknown *a priori* but assumed to be large relative to the layer thickness, H, so that $\varepsilon \ll 1$. We expand the variables

in ε: $c' = c'_0 + \varepsilon^2 c'_2 + O(\varepsilon^4)$, $u' = u'_0 + \varepsilon^2 u'_2 + O(\varepsilon^4)$, $v' = v'_0 + \varepsilon^2 v'_2 + O(\varepsilon^4)$, and $p' = p'_0 + \varepsilon^2 p'_2 + O(\varepsilon^4)$. The scaled, vertically averaged concentration equation (B 1) to $O(\varepsilon^2)$ is

$$Ra\left[\frac{\partial}{\partial\tau}(\overline{c'_0} + \varepsilon^2\overline{c'_2}) + \frac{\partial}{\partial\xi}(\overline{u'_0c'_0} + \varepsilon^2\overline{u'_0c'_2} + \varepsilon^2\overline{u'_2c'_0})\right] - \frac{\partial^2}{\partial\xi^2}(\overline{c'_0} + \varepsilon^2\overline{c'_2}) = 0. \quad \text{(B 3)}$$

We obtain c'_0, c'_2 and u'_0 from the unaveraged concentration equation (2.3):

$$O(\varepsilon^0): Ra\frac{\partial(v'_0c'_0)}{\partial\zeta} - \frac{\partial^2 c'_0}{\partial\zeta^2} = 0, \quad \text{(B 4}a\text{)}$$

$$O(\varepsilon^2): Ra\left[\frac{\partial c'_0}{\partial\tau} + \frac{\partial(u'_0c'_0)}{\partial\xi}\right] + Ra\frac{\partial(v'_0c'_2)}{\partial\zeta} + Ra\frac{\partial(v'_2c'_0)}{\partial\zeta} - \frac{\partial^2 c'_0}{\partial\xi^2} - \frac{\partial^2 c'_2}{\partial\zeta^2} = 0, \quad \text{(B 4}b\text{)}$$

and mass conservation equation (2.1):

$$O(\varepsilon^0): \frac{\partial v'_0}{\partial\zeta} = 0, \quad \text{(B 5}a\text{)}$$

$$O(\varepsilon^2): \frac{\partial u'_0}{\partial\xi} + \frac{\partial v'_2}{\partial\zeta} = 0. \quad \text{(B 5}b\text{)}$$

To obtain u'_0, we first solve (B 5) at $O(\varepsilon^0)$ using the boundary condition $v'_0(\zeta = 0, 1) = 0$ to find $v'_0 = 0$. This indicates that the pressure at $O(\varepsilon^0)$ is hydrostatic, and enables us to find u'_0 using Darcy's law:

$$u'_0 = \frac{\partial c'_0}{\partial\xi}\left(\frac{1}{2} - \zeta\right). \quad \text{(B 6)}$$

To obtain c'_0, we solve (B 4) at $O(\varepsilon^0)$ to find $c'_0 = f(\xi, \tau)$; in other words, c'_0 is not a function of ζ. This result makes use of the no-flux boundary conditions at $\zeta = 0, 1$. To obtain c'_2, we solve (B 4) at $O(\varepsilon^2)$, using (B 5) at $O(\varepsilon^2)$ to simplify the advective part and (B 3) at $O(\varepsilon)$ to remove the time derivative. Requiring $\overline{c'_2} = 0$, we find

$$c'_2 = \frac{Ra}{2}\left(\frac{\partial c'_0}{\partial\xi}\right)^2\left(-\frac{1}{12} + \frac{\zeta^2}{2} - \frac{\zeta^3}{3}\right). \quad \text{(B 7)}$$

We now evaluate the average advective fluxes in (B 3): $\overline{u'_0c'_0} = \overline{u'_0}c'_0 = 0$ and $\overline{u'_2c'_0} = \overline{u'_2}c'_0 = 0$ since the average lateral velocity is always zero. This can be seen by averaging the mass conservation equation (2.1) and using the boundary conditions $u'(\xi \to \pm\infty) = 0$ to find $\overline{u'} = 0$. The remaining advective flux is

$$\overline{u'_0c'_2} = -\frac{Ra}{120}\left(\frac{\partial c'_0}{\partial\xi}\right)^3. \quad \text{(B 8)}$$

We now substitute this expression into (B 3) and replace c_0 using $c_0 = \overline{c} + O(\varepsilon^4)$:

$$Ra\left[\frac{\partial\overline{c'}}{\partial\tau} - \varepsilon^2\frac{Ra}{120}\frac{\partial}{\partial\xi}\left(\left[\frac{\partial\overline{c'}}{\partial\xi}\right]^2\frac{\partial\overline{c'}}{\partial\xi}\right)\right] - \frac{\partial^2\overline{c}}{\partial\xi^2} + O(\varepsilon^4) = 0. \quad \text{(B 9)}$$

This is the scaled version of the equation for Taylor slumping (3.8).

REFERENCES

ASCHER, U. M., RUUTH, S. J. & SPITERI, R. J. 1997 Implicit–explicit Runge–Kutta methods for time-dependent partial differential equations. *Appl. Numer. Maths* **25**, 151–167.

BARENBLATT, G. I. 1952 On some unsteady motions of fluids and gases in a porous medium. *Prikl. Mat. Mekh.* **16**, 67–78, English translation in *Appl. Math. Mech*.

BARENBLATT, G. I. 1996 *Scaling, Self-Similarity, and Intermediate Asymptotics*. Cambridge University Press.

BEAR, J. 1972 *Dynamics of Fluids in Porous Media*. Elsevier, reprinted with corrections, Dover, 1988.

CRANK, J. 1980 *The Mathematics of Diffusion*. Oxford University Press.

DE JOSSELIN DE JONG, G. 1981 The simultaneous flow of fresh and salt water in aquifers of large horizontal extension determined by shear flow and vortex theory. *Proc. Euromech.* **143**, 75–82.

DENTZ, M., TARTAKOVSKY, D. M., ABARCA, E., GUADAGNINI, A., SANCHEZ-VILA, X. & CARRERA, J. 2006 Variable-density flow in porous media. *J. Fluid Mech.* **561**, 209–235.

DUSSAN, V. & AUZERAIS, E. B. 1993 Buoyancy-induced flow in porous media generated near a drilled oil well. Part 1. The accumulation of filtrate at a horizontal impermeable boundary. *J. Fluid Mech.* **254**, 283–311.

ENNIS-KING, J. & PATERSON, L. 2005 Role of convective mixing in the long-term storage of carbon dioxide in deep saline formations. *SPE J.* **10** (3), 349–356.

ERDOGAN, M. E. & CHATWIN, P. C. 1967 The effects of curvature and buoyancy on the laminar dispersion of solute in a horizontal tube. *J. Fluid Mech.* **29** (3), 465–484.

HENRY, H. R. 1964 Effects of dispersion on salt encroachment in coastal aquifers. *Tech. Rep.* 1613-C. USGS.

HESSE, M. A., TCHELEPI, H. A., CANTWELL, B. J. & ORR, F. M. 2007 Gravity currents in horizontal porous layers: transition from early to late self-similarity. *J. Fluid Mech.* **577**, 363–383.

HUPPERT, H. E. & WOODS, A. W. 1995 Gravity-driven flows in porous layers. *J. Fluid Mech.* **292**, 55–69.

LAKE, L. 1989 *Enhanced Oil Recovery*. Prentice Hall.

LAMBERT, J. D. 1991 *Numerical Methods for Ordinary Differential Systems: The Initial Value Problem*. Wiley.

LANDMAN, A. J. & SCHOTTING, R. J. 2007 Heat and brine transport in porous media: the Oberbeck–Boussinesq approximation revisited. *Transp. Porous Med.* **70**, 355–373.

LEVEQUE, R. J. 2002 *Finite Volume Methods for Hyperbolic Problems*. Cambridge University Press.

DE LOUBENS, R. & RAMAKRISHNAN, T. S. 2011 Analysis and computation of gravity-induced migration in porous media. *J. Fluid Mech.* **675**, 60–86.

LYLE, S., HUPPERT, H. E., HALLWORTH, M., BICKLE, M. & CHADWICK, A. 2005 Axisymmetric gravity currents in a porous medium. *J. Fluid Mech.* **543**, 293–302.

MACMINN, C. W., SZULCZEWSKI, M. L. & JUANES, R. 2011 CO_2 migration in saline aquifers. Part 2. Capillary and solubility trapping. *J. Fluid. Mech.* **688**, 321–351.

NGUYEN, N. 2011 *Micromixers: Fundamentals, Design and Fabrication*. Elsevier.

NORDBOTTEN, J. M. & CELIA, M. A. 2006 Similarity solutions for fluid injection into confined aquifers. *J. Fluid Mech.* **561**, 307–327.

PASTER, A. & DAGAN, G. 2007 Mixing at the interface between two fluids in porous media: a boundary-layer solution. *J. Fluid Mech.* **584**, 455–472.

RIAZ, A., HESSE, M., TCHELEPI, H. A. & ORR, F. M. Jr. 2006 Onset of convection in a gravitationally unstable, diffusive boundary layer in porous media. *J. Fluid Mech.* **548**, 87–111.

SMITH, R. 1976 Longitudinal dispersion of a buoyant contaminant in a shallow channel. *J. Fluid Mech.* **78** (4), 677–688.

SZULCZEWSKI, M. L., MACMINN, C. W., HERZOG, H. J. & JUANES, R. 2012 Lifetime of carbon capture and storage as a climate-change mitigation technology. *Proc. Natl Acad. Sci. USA* **109** (14), 5185–5189.

TARTAKOVSKY, D. M., GUADAGNINI, A., SANCHEZ-VILA, X., DENTZ, M. & CARRERA, J. 2004 A perturbation solution to the transient Henry problem for sea water intrusion. In *Developments in Water Science*, vol. 55, pp. 1573–1581. Elsevier.

TAYLOR, G. I. 1953 Dispersion of soluble matter in solvent flowing slowly through a tube. *Proc. R. Soc. Lond.* A **219** (1137), 186–203.

VELLA, D. & HUPPERT, H. E. 2006 Gravity currents in a porous medium at an inclined plane. *J. Fluid Mech.* **555**, 353–362.

YORTSOS, Y. C. 1995 A theoretical analysis of vertical flow equilibrium. *Transp. Porous Med.* **18** (2), 107–129.